Materials Physics and Mechanics. 2023;51(4): 50-65
Research article
http://dx.doi.org/10.18149/MPM.5142023_5

Submitted: November 30, 2022
Approved: May 1, 2023
Accepted: June 13, 2023

Study of burnishining effect on the thermal spray coatings

A. Agnihotri [1] ✉, S.B.S Kalsi [2], H. Kansal [3]

[1] Khalsa College of Engineering and Technology Amritsar, Punjab, India

[2] I. K. Gujral Punjab Technical University Kapurthala, Punjab, India

[3] University Institute of Engineering and Technology, Panjab, India

✉ er.atul84@gmail.com

Abstract. The present study is focused on the protection of alloys against hot corrosion by burnishing the thermal spray coatings. The research study aims to appraise the hot corrosion behavior of WC-Co coatings deposited on boiler steel SA213-T11 using a High-Velocity Oxy-Fuel process (HVOF) followed by a burnishing process. This study also aims to develop a suitable protective burnished-coated material system to enhance the life of metals and alloys operating under a hot corrosion environment. Therefore, the performance of the thermal spray coating followed by the burnishing process is required to be studied for the primary modes of degradation against oxidation and hot corrosion modes of material failure. Various microstructural and mechanical characterizations techniques such as X-Ray Diffractometry (XRD), Scanning Electron Microscopy (SEM), Optical Microscopy, and Microhardness tester were employed to evaluate coating properties. The performance of the thermal spray coating followed by the burnishing process is studied for the primary modes of degradation against oxidation and hot corrosion modes of material failure.
Keywords: HVOF; burnishing; WC-Co; thermal spray coatings

Citation: Agnihotri A, Kalsi SBS, Kansal H. Study of burnishining effect on the thermal spray coatings. *Materials Physics and Mechanics.* 2023;51(4): 50-65. DOI: 10.18149/MPM.5142023_5.

Introduction

Hot corrosion. Presently, alloys are put forth to enhance the utility life span of steam generators, superheaters, etc primarily in the superheated zones of recently brewed ultra-supercritical boilers. Combustion gases create an intemperate atmosphere, and hot corrosion is inevitable when metals are heated for long periods.. Deterioration of the properties of alloys while working under extreme temperature conditions and critical pressure leads to an untimely and premature degradation of metallic components with the cognate endangerment of plant shutdown resulting in the loss in economy, rise in environmental pollution and anticipating the human lives risk. The materials exercised for high-temperature purposes are subjected to high-temperature wear and hot corrosion [1]. Hot corrosion results in the deterioration and subsequent catastrophe of mechanical components and their systems operating in both manufacturing and processing industries thereby affecting their service life expectancy [2]. Hot corrosion has become a very serious problem nowadays in the Power plant equipment industry, which cannot be neglected. Generally, it is observed in hot sections of boilers, gas turbines, coal gasification plants, diesel engines, and incinerators [3]. Many Ferritic sheets of steel are reported to endure high depletion rates under fluidized-bed conditions due to erosion-corrosion [4]. Engineers and researchers have given more intension to this phenomenon when

very severe corrosion was observed in the gas turbine engines of military aircraft during the Vietnam conflict [5].

Preventive measures. In many technical applications, alloy material components must withstand high temperatures, harsh chemicals, erosion, corrosion, and oxidation [6]. It is difficult to arrest corrosion entirely but it can be scaled down significantly using convenient and well-suited anticipatory protective measures. Surface modification and upgrades are needed to protect these components from various deprivations [7]. Protective coatings are the most effective, reliable, and economically possible way to avoid superheater and re-heater hot corrosion [8]. The enhancement in manufacturing technology alone is not enough to reduce the cost issue [9]. Koch et al. [10] reported that corrosion disbursements can be retained approximately by 25-30 % yearly with appropriate preventive measures by controlling hot corrosion. Efforts to reduce the maintenance costs of components employed under high-temperature conditions have raised the awareness of shielding them with protective coatings among researchers [8]. Theemployment of protectivcoatings are the utmost effective, trustworthy, and economically feasible mode to curb or prevent the hot corrosion problems of superheater and re-heater boilers.

High-velocity oxy-fuel process. Thermal spray coatings augment the lifespan of components that operate at extreme temperature conditions. The application of thermal sprayed coatings is found to be a unique, practical, reliable, and economically feasible way to control or avoid hot corrosion [11–13]. The high-velocity oxy-fuel (HVOF) process of coatings is regarded as the "most popular thermal spraying technology" [9]. HVOF spraying is a fast-growing method for treating high-temperature corrosion, challenging the costly vacuum plasma spraying technique (VPS). The HVOF method of spraying has been adopted by several thermal spray industries because of its "cost-effectiveness", flexibility, and exceptional coating quality. The coatings generated by this process exhibit higher bond strength and hardness value along with low porosity as compared to other thermal spraying processes such as plasma spraying, flame spraying, and arc spraying [14]. The HVOF thermal spray method of coatings is widely employed in several applications including gas turbines, paper and pulp, petroleum, chemical, automotive industries, and energy-conversion [1,9]. These are also applied in manufacturing industries, boilers, superheaters, reheaters, pipe systems, and valve bodies [15,16]. HVOF thermal spraying deposits a coating with smaller porosity, better bond strength, greater hardness, and less decarburization [17]. HVOF is used in aviation, automobile, marine, and petrochemical process components. Sidhu et al. [9] reported that HVOF coating had lower roughness, porosity, and oxide content than conventional thermal coating methods.

Burnishing process on the applied coating. The protection provided by the coating against hot corrosion depends upon many factors. But one very important factor is the porosity of thermal sprayed coating because corrosion species travel through these pores to the substrate. Still, even with the advancement in thermal spray technologies, it is impossible to attain pores-free thermal spray coatings. Some voids are always formed at the splat boundaries during the thermal spray coating process and corrosion species penetrate through the voids [18]. Various researchers had employed the post-treatment process to deposit coatings to reduce their porosity value. A mechanical process known as ‘burnishing’ is used as a super finishing treatment for metallic components. In this process, a super-finished and hardened material in the form of a roller or ball is allowed to move over the surface of the component with the application of some pressure. This results in the elastic-plastic deformation of the component surface. The rolled surface gets finished and its porosity reduces to a greater extent. Luca et al. [19] opined that in addition to constructing a good surface finish, the burnishing process also improved the other properties of the material such as hardness, corrosion resistance, and fatigue life. The Burnishing process is used to achieve a high surface finish on metals resulting in a smooth hardened surface with some improved mechanical properties [20].

Burnishing as a novel approach can be employed in this research study to reduce the porosity of thermal spray coating. The research study aims to determine the effect of burnishing on thermal spray coatings against high-temperature aggressive environmental applications of boilers, gas turbines, waste-to-energy plants, etc. This study also aims to develop a suitable protective burnished-coated material system to enhance the life of metals and alloys operating under a hot corrosion environment.

Materials and Methods

Substrate Metal Alloys. The substrate base metal alloys selected for the present study are "ASTM-SA213-T-11" (T11). This alloy is utilized as a boiler tube material in the "Power Plants situated in North India". The substrate alloy was provided by "Cheema Boilers Private Limited" (India) in the rolled sheet form for research purposes to examine their protective behavior against high temperature corrosive environmental conditions. Nominal and actual chemical compositions of these alloys along with their applications are provided in Table 1.

Table 1. Nominal and actual composition along with an industrial application of T11 alloy

Alloy	Composition	Chemical composition, wt. %							
		C	Mn	Si	S	P	Cr	Mo	Fe
SA213-T11	Nominal	0.15	0.3-0.6	0.5-1	0.03	0.03	1-1.5	0.44-0.65	Bal.
	Actual	0.1369	0.4292	0.3038	0.0065	0.0124	0.9114	0.5125	Bal.

Feedstock Powders for Coating. The commercially available WC-Co feedstock material in a powdered form have been utilized as the coating powder to be deposited on base metal substrate alloys for appraising their hot-corrosion performance at high-temperature conditions. The chemical composition and size of particles of these feedstock materials are given in Table 2.

Table 2. Composition of feedstock powders

Feedstock alloy	Chemical composition, wt. %	Shape	Nominal composition	Weight percentage, %
WC-Co powder	80WC- 20Co	Spherical	Tungsten carbide	Base
			Total Carbon	5.3-5.4
			Cobalt	11-13

Table 3. Spray parameters employed for HVOF coating

Parameters	Gun DJH 2600 & Nozzle DJH 2603
Oxygen flow rate, SLPM*	14-16
Fuel (LPG) flow rate, SLPM	26-31
Air flow rate, SLPM	33
Spraying distance, inch	9
Fuel pressure, kg/cm^2	8-10
Oxygen pressure, kg/cm^2	12
Air pressure, kg/cm^2	9
Feed rate, gm/min	50-60

* SLPM =Standard Liters Per Minute

Development of Coatings. The boiler steel alloys were sectioned and specimens were cut to the dimensions of 20 × 15 × 5 mm The dimensioned specimens were abraded down with silicon carbide papers to 180 grit. Then, these specimens underwent sandblasting by alumina (Grit 45) preceding the application of coatings. This task is performed to obtain healthier adhesion between coating and substrate. The utmost attention was considered to evade any sort of structural changes in all physically formulated. The coatings were thermally sprayed at Spraymet Surface Technologies Private Limited, Bengaluru (India) utilizing High-velocity

oxy-fuel (HVOF) thermal spray systems. The spraying parameters engaged while thermal spraying are given in Table 3.

Post-treatment of coating by burnishing process. In this study, the coated specimens underwent a burnishing process by high strength roller as the burnished tool was affixed to the Shaper machine. Burnishing is done with a force of 60 N at a constant speed of 200 rpm for 50–60 passes at a feed rate of 0.05 mm/rev. Figure 1 depicts the specimens' burnishing.

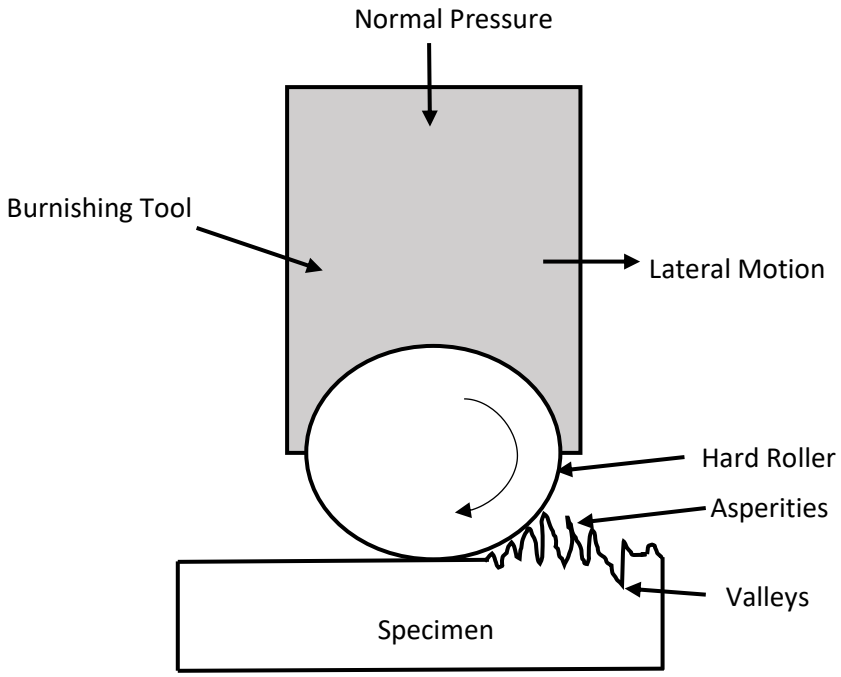

Fig. 1. Burnishing technique

Experimentation. As-sprayed specimens and burnished-coated specimens were cold mounted in the cold-setting epoxy compound along their surface. Then the specimens were polished with 220, 400, and 600 grate silicon carbide emery papers having 1/0, 2/0, 3/0 and 4/0 grades and subsequently polished on the wheel polishing machine with 1 μm alumina powder suspension. As-sprayed and burnished-coated specimens were then cross-sectioned through a low-speed diamond cutter (Buehler's Precision Diamond Saw, Model: ISOMET 1000, Make: USA) for their cross-sectional analysis. The cross-sectioned specimens were cold-mounted using an epoxy cold-setting compound along their cross-section. Subsequently, these specimens were polished according to a similar procedure as explicated for surface preparation. These specimens were then cross-sectioned through a low-speed diamond cutter (Buehler's Precision Diamond Saw, Model: ISOMET 1000, Make: USA) for their cross-sectional analysis. The cross-sectioned specimens were cold-mounted using an epoxy cold-setting compound along their cross-section. Subsequently, these specimens were polished according to a similar procedure as explicated for surface preparation. The formulated specimens were polished to expose their coating microstructure and their porosity is analyzed by an Image Analyser System using PMP3 Inverted Metallurgical Microscope (Make: Japan) incorporated with Material Plus software based on ASTM standards. The surface morphologies and cross-sectional microstructures of these specimens were obtained by an Inverted Optical Microscope (Model: Axiovert-200 MAT, Make: Carl Zeiss, Germany) conjugated with the Imaging software (Zeiss Axio Vision, Germany). The microhardness values of all specimens across their cross-section were assessed by a Microhardness Tester (Miniload 2, Make: Germany) equipped with Vickers Pyramidal Diamond Indenter.

Results

Scanning electron microscopy (SEM) and X-ray diffractometry (XRD) analysis. SEM morphology of WC-Co feedstock powders shows its spherical morphology as shown in Fig. 2. The diffraction patterns for the WC-Co powder is shown in Fig. 3 on the moderated scale. In the W-Co-C system, WC and W_2C double carbides, are the most stable phases. The principal phase comprising Co-based fcc for WC-Co powder specifies the formation of a solid solution. Reduction in the amount of carbon in WC-Co alloys causes the WC carbide to convert into W_2C carbides.

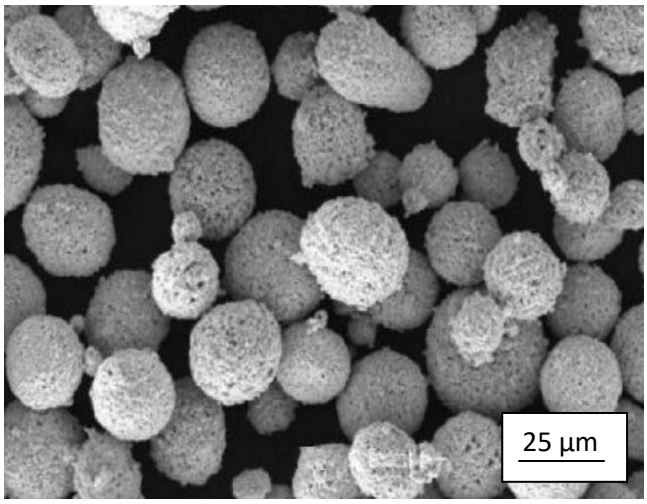

Fig. 2. SEM images of powder WC-Co

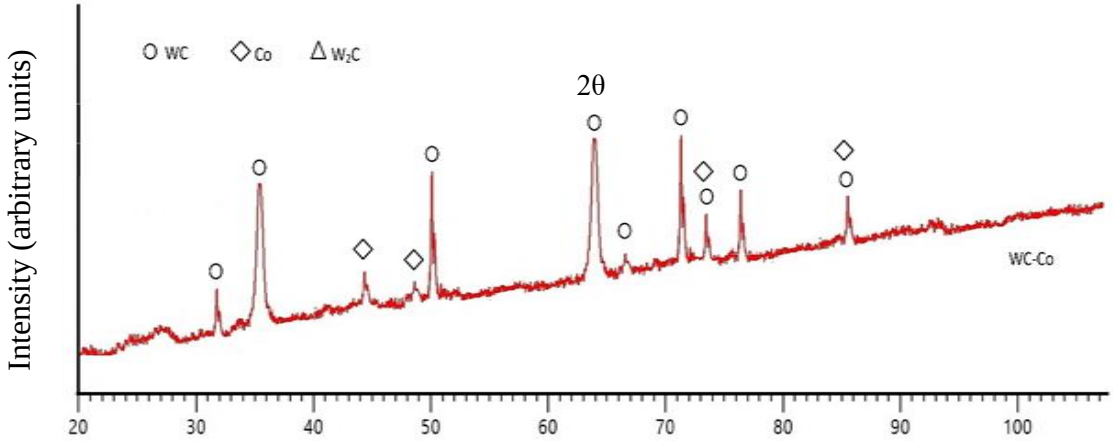

Fig. 3. XRD patterns for the HVOF feedstock WC-Co coating powder

Substrate alloys. The optical microstructures of substrate materials under the present research study are shown in Fig. 4. The microstructures of selected substrates have been characterized by assessing them with comparable international standard superalloys as presented in ASM and Metals Handbooks. These substrates steel are generally signified as 'ferritic' low alloy steels which exhibit a bainite microstructure [21]. This microstructure ensures the finest creep resistance, while its extensive period usage and assessing strength is governed by fine precipitates present inside that microstructure. Chromium presence in these substrates not only enhances the property of the resistance against oxidation but also retards the transformation on cooling from austenite i.e. martensite becomes the predominant microstructure. While tempering, Mo_2C which is the most stable carbide gets formed having low nucleation energy. Mo_2C configuration has needle-shaped fine particles which develop

gradually at normal servicing temperature as a result of a great coherency among the lattice configurations of carbide particles and enclosing ‘ferrite’ matrix [22].

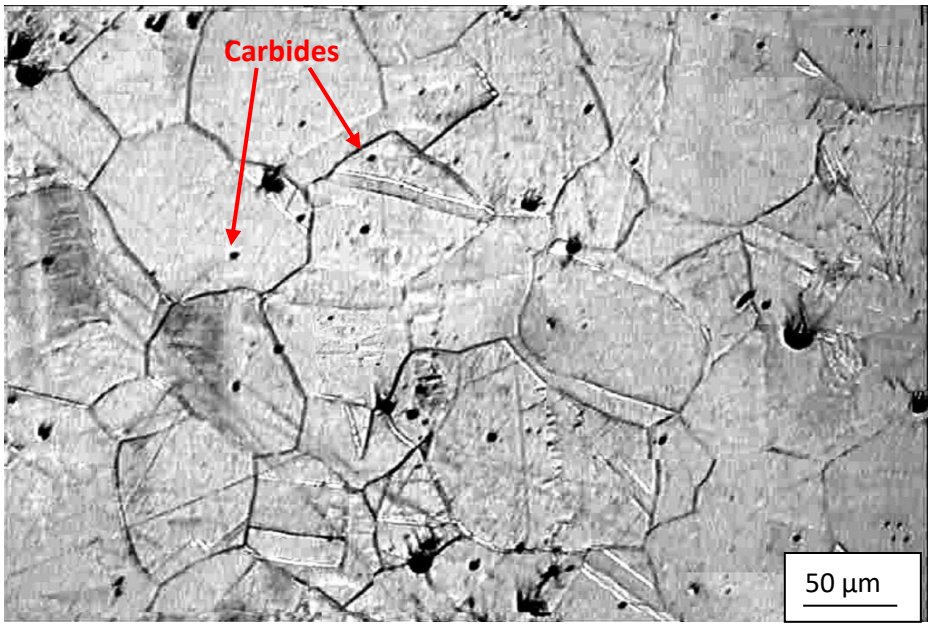

Fig 4. Optical micrographs of SA213-T11 substrate

Coated alloys. Visual Examinations. Optical micrographs of the as-sprayed specimens are shown in Fig. 5. It can be noticed that as-sprayed WC-Co coatings exhibit a shining silver-grey color. After burnishing, the same specimens indicate a dull deep grey appearance. Visual observations also show that as-sprayed coating has smooth surfaces, whereas after burnishing the coated specimen has a rough surface. Further, no surface cracks were found on any coatings surface. A surface recorder of resolution 0.008 µm "SE-1200, Kosaka Laboratory Ltd., Tokyo, Japan" were used to measure surface roughness values which came in the range of 4-6 µm.

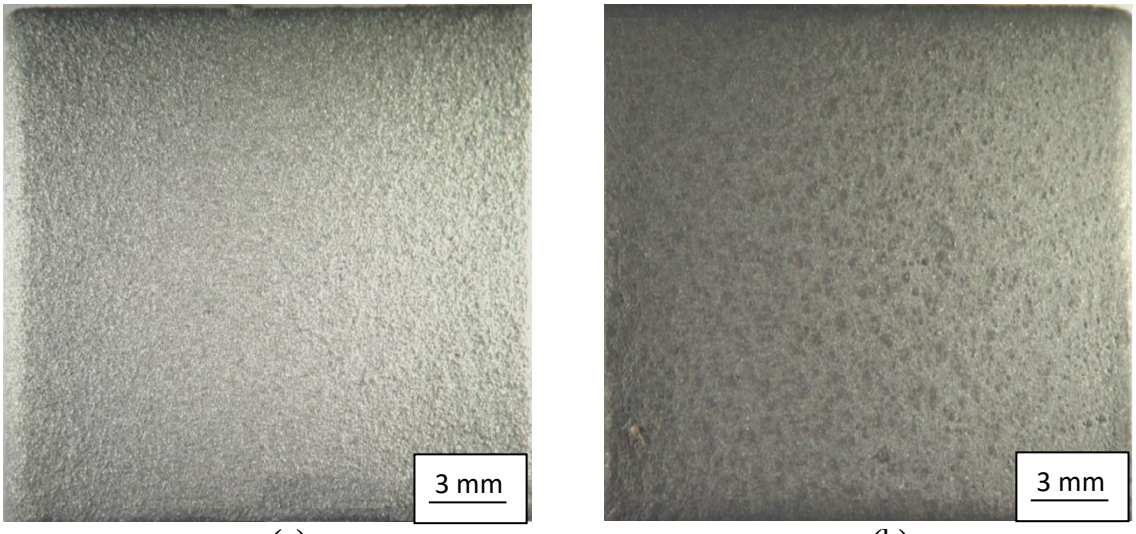

(a) (b)

Fig. 5. Optical micrographs of as-sprayed coatings on substrate T11 with (a) WC-Co coating; (b) burnished WC-Co coating

Measurements of Coating Thicknesses. The coating thickness was determined from Back scattered electron images (BSEI) obtained along the cross-section of coated specimens. The average thickness of the burnished coated specimen is 280 µm and WC-Co coated specimen is 290 µm off. The BSE image for burnished WC-Co-coated WC-Co-coated specimen for representation is shown in Fig. 6.

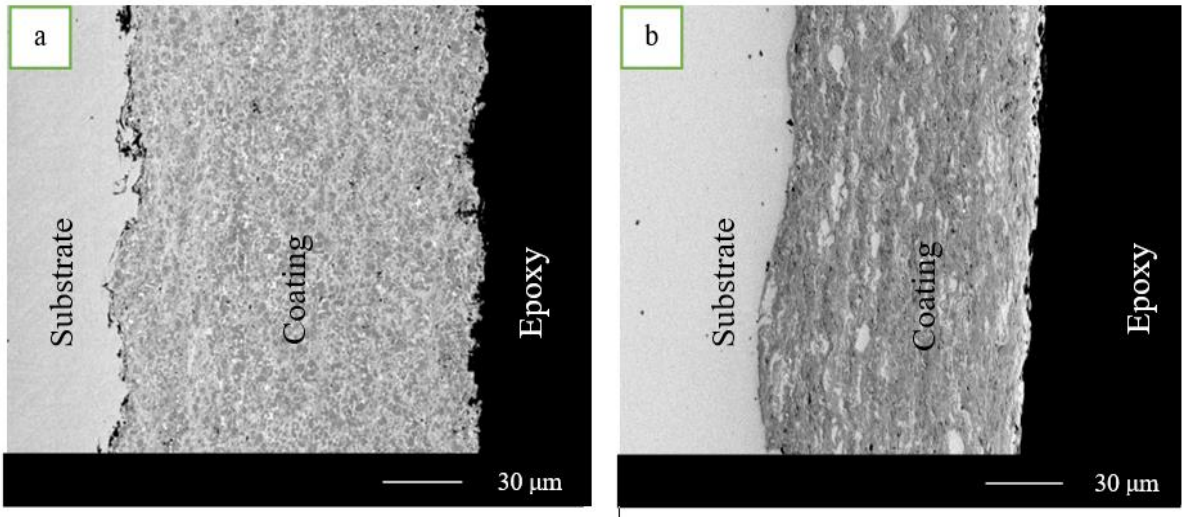

Fig. 6. BSEI micrographs showing cross-section morphologies of different HVOF coatings on: (a) burnished WC-Co coating on T11; (b) WC-Co coating on T11

Porosity Analysis. The area of pores in a view field was analyzed with an analyzing software in which the grey area of pores transform into a red background while the rest microstructure persists in its primary color. The area of one feature is statistically interrelated to the overall area of the image, as the software reckons the number of pixels of one color type (red) and establishes that as a proportion of the over-all number of pixels in an image (entire area). Five readings of porosity values have been assessed for each specimen. The average porosity of burnished coatings and as-sprayed coatings of specimens are observed to be less than 1.2 and 2 % respectively.

Microhardness measurements. Microhardness profiles along the cross-section of coatings as a function of distance from the interface of coating-substrate are shown in Fig. 7. The hardness value of substrate T11 is observed in the range of 310 to 400 HV. The hardness of the burnished WC-Co coated specimen is 919-999 HV, while the hardness of the WC-Co coated specimen is on the order of 630 HV.

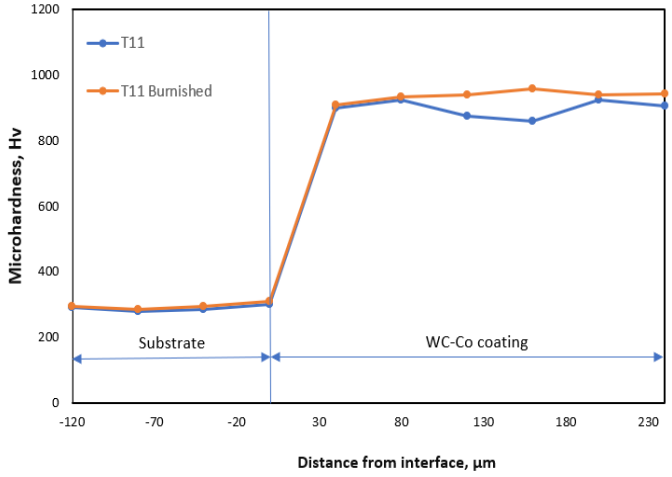

Fig. 7. Microhardness profiles for T11 substrate with WC-Co coating

Metallographic studies of WC-Co the coatings. Surface microstructure of coating. The optical micrographs of WC-Co coating and burnished coatings on T11 substrates selected for the present study are shown in Fig. 8. The irregularly shaped flat splats appear to be uniformly dispersed in the coating. The white globules distributed throughout the structure appear as melted regions. Some unmelted particles and limited voids are also observable in the coating structure. The un-melted particles in the coating structures are identified by their surface morphology including shape and size.

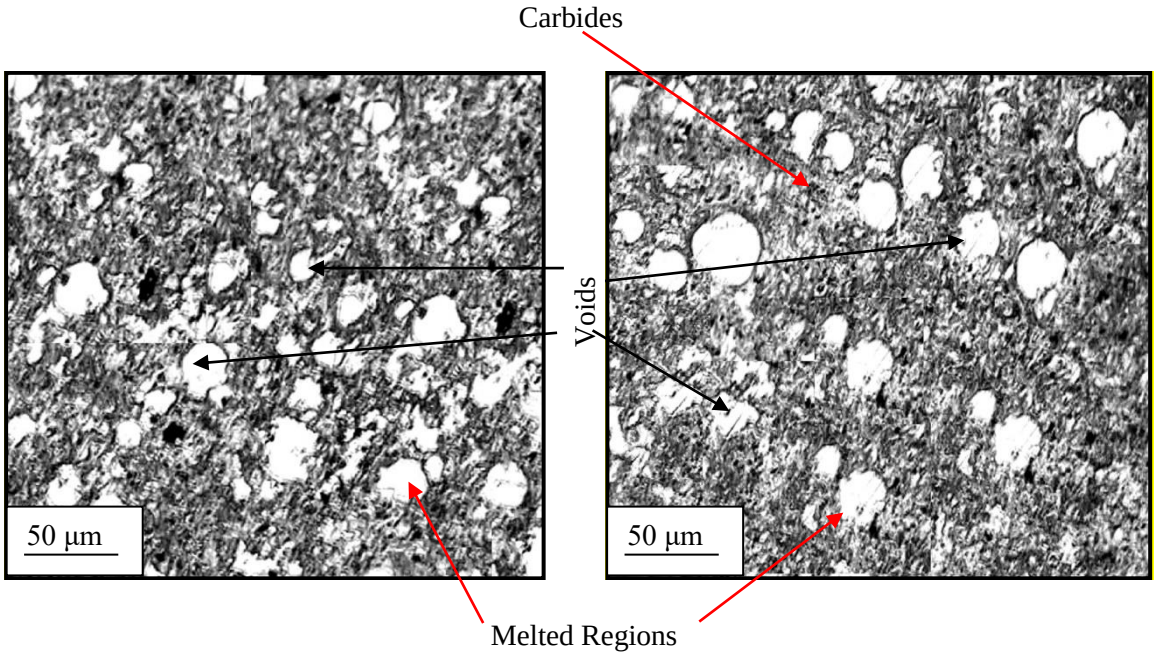

Fig. 8. Optical micrographs displaying surface morphology of WC-Co coating on substrate: (a) T11 and (b) T11 burnished

Cross-Section Microstructures. Optical micrographs displaying WC-Co coatings having cross-sectional microstructure are shown in Fig. 9. WC-Co coating has a relatively fine grain microstructure including white globules disbursed all over the structure.

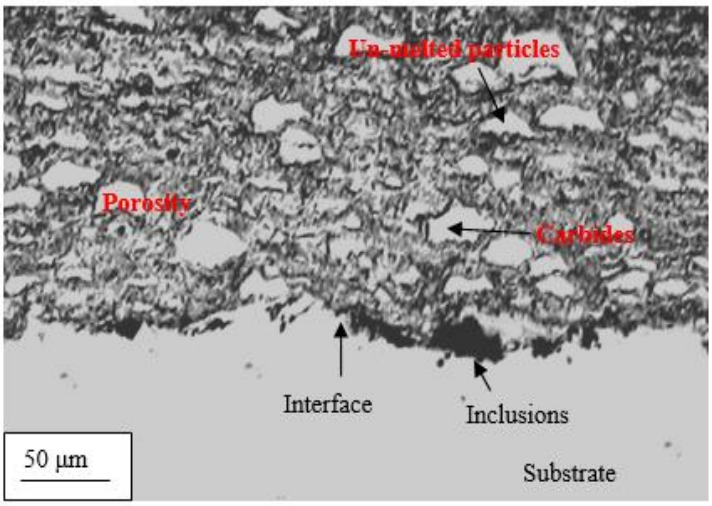

Fig. 9. Optical micrographs displaying cross-sectional microstructures of WC-Co coating

X-ray diffractometer study. XRD pattern on a reduced scale for the as-sprayed WC-Co coating is shown in Fig. 10. The presence of WC-based fcc as the principal phase for the selected as-sprayed coatings signifies the establishment of a solid solution matrix.

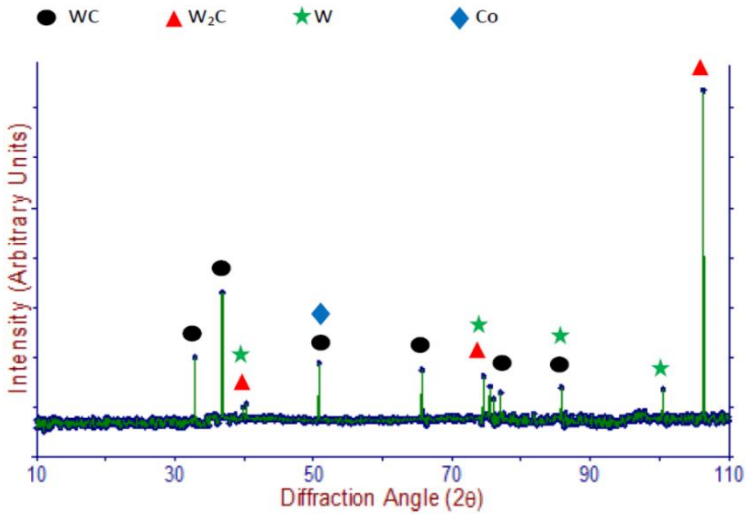

Fig. 10. Diffraction patterns for "WC-Co coatings" on T11

SEM analysis. SEM morphologies for WC-Co and burnished WC-Co coatings deposited over the T11 substrates are shown in Fig. 11(a) and 11(b) respectively. As evident from the micrographic features, the coatings are homogeneous and substantial as well as free from cracks.

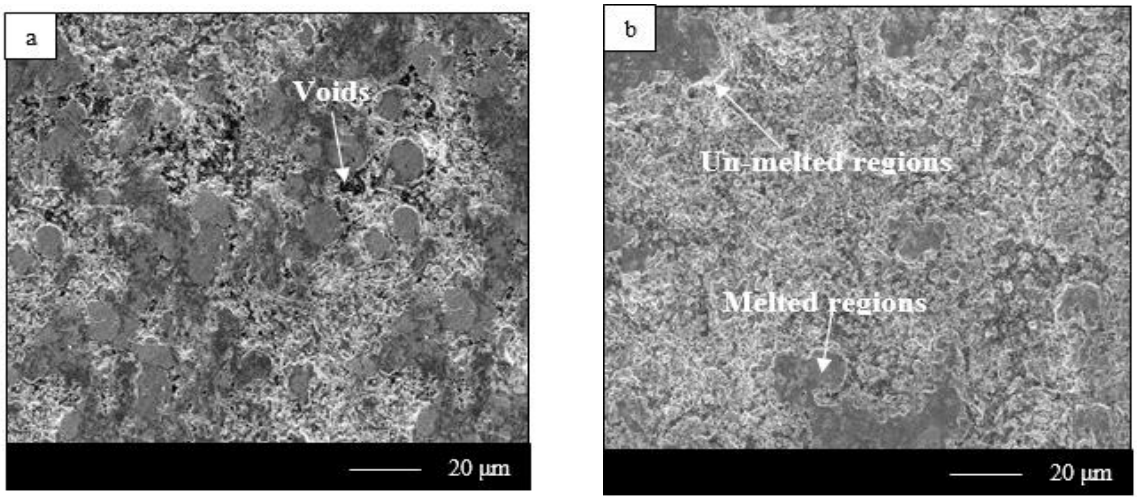

Fig. 11. Surface morphology displayed by SEM micrographs for WC-Co coating on substrates: (a) T11; (b) T11 burnished

A minimal number of unmelted particles are spotted in the structure of the coating. These unmelted particles may adhere to the substrate surface due to high impact while HVOF spraying. The coatings exhibit the presence of certain oxide inclusions and very limited open pores. Further, some localized areas which have greater densities of open pores are also observed in some micrographs. However, the burnishing technique covers the open pores to a larger extent. Surface morphologies disclosed the crystalline structures of all coatings deposited on the substrates. The burnished coated specimen has small size splats, whereas medium-sized splats are noticed in the case of the applied coating.

Energy-dispersive X-ray analysis. Energy-dispersive X-ray (EDAX) analysis of the WC-Co coated specimen was done at selected spots, as shown in SEM micrographs shown in Fig. 12. The melted and partly melted regions as well as black areas are clearly distinguished in WC-Co coating. Partially molten state regions contain 87 % tungsten carbide and 11 % cobalt, which is nearby to the composition of WC-Co coating powder. The black regions visible in this coating seem to WC dominant.

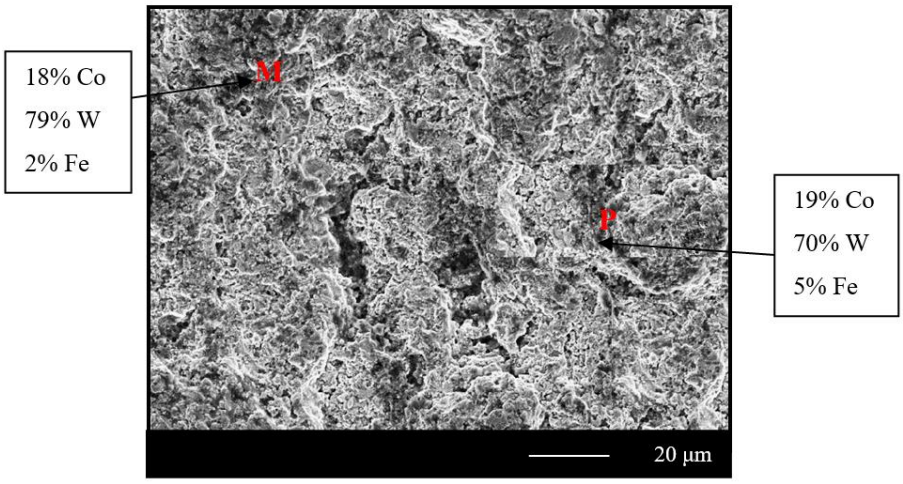

Fig. 12. Elemental composition (wt. %) at selected points analyzed by EDAX for WC-Co coating indicating elemental composition (wt. %) at selected points

Cross-section analysis. Back scattered electron (BSE) images shown in Fig. 13 were taken across the cross-section of coated as well as a burnished-coated specimen for their cross-sectional investigation. In WC-Co coated specimen, the weight percentage of iron shows a slight drop i.e. from 43.9 to 41.49 % while the chromium weight percentage increases from 32 to 35.6 % which is slightly greater than the nominal composition of the substrate.. BSE Images and EDAX study at point 2 and point 4 indicate that the distinguish matrix phase has a similar composition as the coating powder. At location 3, the white phase of chromium-rich splat is observed.

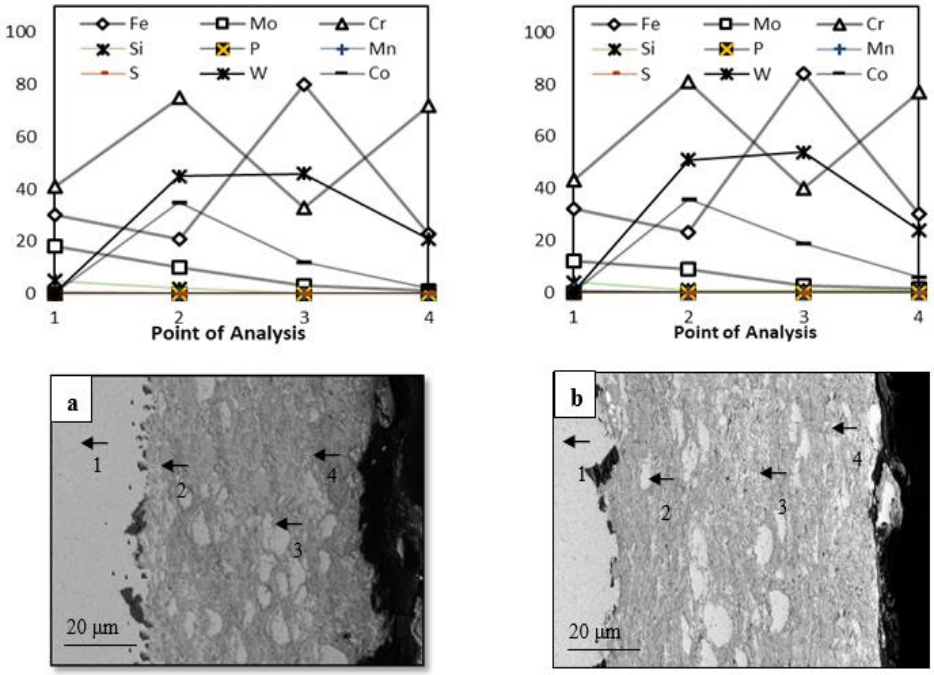

Fig. 13 Cross-sectional EDAX analysis (wt. %) of WC-Co coated specimens for: (a) T11 and (b) burnished-coated T11

Discussion

Both the specimens i.e. under analysis have a solid suspension matrix. The consistent presence of carbides was noticed in all the selected specimens. The strength of these chromium-based specimens depends upon the mechanism of precipitation hardening, in addition to the solid solution hardening. The burnishing technique on the specimen also increases the surface hardness of the specimen comprehensively. Different types of carbides formed due to precipitation with the assistance of various elements present in the superalloy. WC has the greatest possibility of formation in all specimens since it is primarily promoted by the tungsten [23]. Further, W_2C carbide tends to precipitate at the grain boundaries [24]. Some large globules observed in Fig. 4 signify the presence of the WC phase. Thicker coatings show better resistance against corrosion [25]. However, the self-disintegration of thicker coatings limits the thickness of the coatings [26]. Therefore, the deposition of 280-298 μm thick HVOF coating on substrates was selected in the present research study to certify the integrity of the coating [27]. The thickness of coating evaluated along the cross-section of specimens has been attained to the required extent of 280-298 μm as mentioned earlier in the study. HVOF coatings have a comparatively smooth as-sprayed surface finishing with surface roughness ranging between 4-6, as observed in Fig. 5. In HVOF coatings, high-impact energy is imposed upon the impinging particles. This cause a better mechanical bonding of sprayed particles for developing a homogenous structure thereby requiring less finishing compared to the other thermal spraying techniques.

Porosity is regarded as the most significant property of the coatings tested under high-temperature applications of hot-corrosion environments. Materials with larger porosity have lower mechanical strength because the connection between the particles and the matrix weakens as porosity rises. The corrosive species can penetrate through the porosities (preferred corrosion paths) to approach the surface of the substrate thereby resulting in a prompt attack of corrosion. Dense coatings have a very low value of porosity and therefore, impart better resistance against corrosion [28]. The as-sprayed HVOF coatings have lesser porosity because of the greater momentum of feedstock material powder particles. The uniformly flat disc powder particles tremendously adhere to the substrate surface producing a very dense coating structure. The appraised porosity values of the applied coatings are similar to the results of [29–34].

Hardness has been regarded as the most common mechanical property of the coating. The erosion-corrosion degradation conduct of coatings is generally affected by their hardness value [35]. Noteworthy observations have been made after examining the microhardness profiles in detail. As noticed in Fig. 7, the substrate region adjacent to the coating-substrate boundary indicated a higher hardness value than their core region. The augmented hardness value adjoining the coating-substrate interface is attributed to the "strain-hardening effect" due to the execution of abrasive blasting over the substrate surface before the deposition of [36]. The higher hardness value of coating is also contributed by the "high impact speed" of coating droplets while HVOF spraying results in superior density as well as better cohesive strength of distinct splats [34–37].

The microhardness of the applied coatings in a present research study is ascertained to be much better than the substrate alloy. The hardness value further gets improved after burnishing the coated specimens [38]. Certain variations in the hardness value of each coating along their cross-section of substrates have been also observed. These differences in the hardness values are due to the presence of permeability, melted, un-melted, and partly melted particles as well as oxide inclusions as shown in the cross-sectional micrographs of coatings in Fig. 9. The microhardness values of HVOF coatings assessed in the present research study are compatible with the outcomes of [39–45]. The insignificant diffusion of substrate elements to the coating also contributes towards the different microhardness values as specified by EDAX analysis.

The coatings micrographs on substrates along their cross-section are shown in Figs. 6 and 9 respectively. Inference can be drawn from the observations that the applied coatings possess uniform dense structures. The coatings also exhibit the layered morphologies of distinctive splats as a result of re-solidification and accumulation of melted or semi-melted precipitations. The long axis of an "impacted splat is orientated parallel to the surface" of the substrate. As observed from the micrographs, the un-melted particles in microstructures are very less in number since the major proportion of the feedstock powders got melted completely or partly before their impact with the substrate. The microstructures have not shown any significant difference between individually applied coating on selected substrate. Microstructures examined in the current investigation are almost comparable to the results of HVOF-applied coatings [46–48].

SEM/EDAX analysis presented in Fig. 12 specifies that HVOF coatings employed under the research study meet the requisite composition. In Fig. 12, the region marked "M" which appears to be featureless, is established by the collision of completely melted feedstock material droplets. Consequently, these droplets got hardened at a high rate of cooling i.e. 10^7 K/s [49] . The microcrystalline structure developed due to a high cooling rate as also reported by [50]. These micro-crystalline grains undergo solidification precisely from the molten state by heterogeneous nucleation on already prevailing oxide granules [51].

As shown in EDAX analysis in Fig. 13, point 4 exhibits the presence of little content of oxygen leading to the oxide phase which specifies that some inadequate oxidation has happened on the surface of the coating or onboard particles before the buildup of the subsequent layer. Similar outcomes regarding oxide growths in HVOF-sprayed coatings have been informed by [52,53]. Certain inclusions of oxides are also spotted in "SEM/EDAX analysis" (Fig. 11) where some inclusions were present consistently among all coatings at the interface of substrate and coating. EDAX analysis in Fig. 13, has indicated the existence of chromium oxide inclusions due to the presence of chromium and oxygen at these points [54].

EDAX results for the HVOF sprayed coatings under research study (as shown in Fig. 12) indicate that there exists an "inter-diffusion of various elements between the substrate and coatings" as evident from Fig. 13. This inter-diffusion mechanism can affect the hot corrosion behavior of any particular coating on different substrates. Chromium and tungsten are observed as the most vulnerable elements to the phenomenon of diffusion. Mo, Fe, Co, and Mn are some of the elements which are susceptible to minor diffusion. The diffusion of elements between the coating and substrate can influence the performance of coating under high-temperature applications [55–56].

Conclusions

The burnishing force increases the wear resistance of the selected specimens. The continuous rolling of the burnishing tool over the surface of specimens leads to their plastic deformation. This results in the work-hardening effect on the surface and it becomes harder than the remaining surface of the specimen. The surface hardness of the material is directly proportionate to the applied strength i.e. an increment in the burnishing force surges the surface hardness of the material. The increment in hardness of the material is attributed to the increase of penetration depth and flow of metal which enhances the extent of deformation of voids present in the metal. The hardness of the disturbed layer of the surface improves significantly when the burnishing process is continuously applied for a longer period on the metal surface. Hence, the burnishing process decreases surface roughness by improving the smoothness of the surface.

References

1. Hao E, Wang Y, Zhao X, Gao M, Chen J, An Y, Yan F. Influence of molten salt with or without V2O5 on hot corrosion and high-temperature tribological performance of HVOF-sprayed Ni-based self-lubricating composite coating. *Surface and Coatings Technology*. 2021;417: 127210.
2. Yu Z, Chen M, Wang J, Li F, Zhu S, Wang F. Enamel coating for protection of the 316 stainless steel against tribo-corrosion in molten zinc alloy at 460° C. *Journal of Materials Science & Technology*. 2021;65: 126–136.
3. Abu-Warda N, López AJ, López MD, Utrilla MV. High temperature corrosion and wear behavior of HVOF-sprayed coating of Al2O3-NiAl on AISI 304 stainless steel. *Surface and Coatings Technology*. 2019;359: 35–46.
4. Faes W, Lecompte S, Ahmed ZY, Van Bael J, Salenbien R, Verbeken K, De Paepe M. Corrosion and corrosion prevention in heat exchangers. *Corrosion Reviews*. 2019;37(2): 131–155.
5. Rapp RA. Hot corrosion of materials. *Pure and Applied Chemistry*. 1990;62(1): 113–122.
6. Binal G. Isothermal oxidation and hot corrosion behavior of HVOF sprayed 80Ni-20Cr coatings at 750° C. *Surface and Coatings Technology*. 2023;454: 129141.
7. Singh S, Goyal K, Bhatia R. A review on protection of boiler tube steels with thermal spray coatings from hot corrosion. *Materials Today: Proceedings*. 2022;56: 379–383.
8. Wang Q, Zhou D, Yu M, Shi L, Li X, Sun Q. Oxidation and hot corrosion behaviors of Mo-doped NiMoAlY alloys at 750° C. *Corrosion Science*. 2022;201: 110262.
9. Sidhu TS, Agrawal RD, Prakash S. Hot corrosion of some superalloys and role of high-velocity oxy-fuel spray coatings—a review. *Surface and Coatings Technology*. 2005;198(1–3): 441–446.
10. Koch GH, Brongers MP, Thompson NG, Virmani YP, Payer JH. *Corrosion cost and preventive strategies in the United States*. United States: Federal Highway Administration; 2002.
11. Zhou W, Zhou K, Li Y, Deng C, Zeng K. High temperature wear performance of HVOF-sprayed Cr3C2-WC-NiCoCrMo and Cr3C2-NiCr hardmetal coatings. *Applied Surface Science*. 2017;416: 33–44.
12. Dzhurinskiy D, Babu A, Pathak P, Elkin A, Dautov S, Shornikov P. Microstructure and wear properties of atmospheric plasma-sprayed Cr3C2-NiCr composite coatings. *Surface and Coatings Technology*. 2021;428: 127904.
13. Singh V, Singh I, Bansal A, Omer A, Singla AK, Goyal DK. Cavitation erosion behavior of high velocity oxy fuel (HVOF) sprayed (VC+ CuNi-Cr) based novel coatings on SS316 steel. *Surface and Coatings Technology*. 2022;432: 128052.
14. Parker DW, Kutner GL. HVOF-spray technology: poised for growth. *Advanced Materials & Processes*. 1991;139(4): 68–74.
15. Wu Q, Zheng H, Zhang Z, Hu P, Fan C, Zhong N, Liu Y. High-temperature wear and cyclic oxidation behavior of (Ti, W) C reinforced stainless steel coating deposited by PTA on a plain carbon steel. *Surface and Coatings Technology*. 2021;425: 127736.
16. Luo K, Li S, Xu G, Hosseini SR, Lu J. Hot corrosion behaviors of directed energy deposited Inconel 718/Haynes 25 functionally graded material at 700° C and 900° C. *Corrosion Science*. 2022;197: 110040.
17. Kaushal G, Singh H, Prakash S. High-temperature erosion-corrosion performance of high-velocity oxy-fuel sprayed Ni-20 Cr coating in actual boiler environment. *Metallurgical and Materials Transactions A*. 2011;42: 1836–1846.
18. Kumar S, Kumar R, Singh S, Singh H, Handa A. The role of thermal spray coating to combat hot corrosion of boiler tubes: a study. *Journal of Xidian University*. 2020;14(5): 229–239.
19. Luca L, Neagu-Ventzel S, Marinescu I. Burnishing of Hardened Steel Components-An Alternative Method of Finishing. *Proceedings of Annual Meeting for American Society for Precision Engineering*. 2001;27: 110–114.
20. Vinitha M, Rao AN, Mallik MK. Optimization of speed parameters in burnishing of samples fabricated by fused deposition modeling. *Int. J. Mech. Ind. Eng*. 2012;2(2): 10–12.

21. Shibli A. Boiler steels, damage mechanisms, inspection and life assessment. In: *Power plant life management and performance improvement*. Woodhead Publishing; 2011. p.272–303.
22. Yamasaki S, Bhadeshia HK. Modelling and characterisation of Mo2C precipitation and cementite dissolution during tempering of Fe–C–Mo martensitic steel. *Materials Science and Technology*. 2003;19(6): 723–731.
23. Davis JR. (Ed.) *ASM specialty handbook: tool materials*. ASM International; 1995.
24. Alhaji A, Shamanian M, Salehi M, Nahvi SM, Erfanmanesh M. Electroless nickel–phosphorus plating on WC–Co powders using HVOF feedstock. *Surface Engineering*. 2019;35(2): 120–127.
25. Heath GR, Heimgartner P, Irons G, Miller RD, Gustafsson S. An assessment of thermal spray coating technologies for high temperature corrosion protection. *Materials Science Forum.* 1997;251: 809–816.
26. Sadeghi E, Markocsan N, Joshi S. Advances in corrosion-resistant thermal spray coatings for renewable energy power plants. Part I: Effect of composition and microstructure. *Journal of Thermal Spray Technology*. 2019;28: 1749–1788.
27. Singh G, Bala N, Chawla V. Microstructural analysis and hot corrosion behavior of HVOF-sprayed Ni-22Cr-10Al-1Y and Ni-22Cr-10Al-1Y-SiC (N) coatings on ASTM-SA213-T22 steel. *International Journal of Minerals, Metallurgy and Materials*. 2020;27: 401–416.
28. Zhao S, Xie X, Smith GD, Patel SJ. The corrosion of INCONEL alloy 740 in simulated environments for pulverized coal-fired boiler. *Materials Chemistry and Physics*. 2005;90(2–3): 275–281.
29. Gil L, Staia MH. Microstructure and properties of HVOF thermal sprayed NiWCrBSi coatings. *Surface and Coatings Technology*. 1999;120: 423–429.
30. Guilemany JM, Fernandez J, Delgado J, Benedetti AV, Climent F. Effects of thickness coating on the electrochemical behaviour of thermal spray Cr3C2–NiCr coatings. *Surface and Coatings Technology*. 2002;153(2–3): 107–113.
31. Faes W, Lecompte S, Ahmed ZY, Van Bael J, Salenbien R, Verbeken K, De Paepe M. Corrosion and corrosion prevention in heat exchangers. *Corrosion Reviews*. 2019;37(2):131–155.
32. Palomino LM, Suegama PH, Aoki IV, Montemor MF, De Melo HG. Electrochemical study of modified non-functional bis-silane layers on Al alloy 2024-T3. *Corrosion Science.* 2008;50(5): 1258–1266.
33. Guilemany JM, Dosta S, Miguel JR. The enhancement of the properties of WC-Co HVOF coatings through the use of nanostructured and microstructured feedstock powders. *Surface and Coatings Technology*. 2006;201(3–4): 1180–1190.
34. Sidhu TS, Prakash S, Agrawal RD. Characterisation of NiCr wire coatings on Ni-and Fe-based superalloys by the HVOF process. *Surface and Coatings Technology*. 2006;200(18–19): 5542–5549.
35. Meghwal A, Matthews S, Howse H, Berndt CC, Ang AS. Steam and air oxidation behaviour of thermal spray chromium carbide-based composite coatings. *International Journal of Refractory Metals and Hard Materials*. 2023;111: 106088.
36. Khan MA, Sundarrajan S, Natarajan S, Parameswaran P, Mohandas E. Oxidation and hot corrosion behavior of nickel-based superalloy for gas turbine applications. *Materials and Manufacturing Processes*. 2014;29(7): 832–839.
37. Sidhu HS, Sidhu BS, Prakash S. Mechanical and microstructural properties of HVOF sprayed WC–Co and Cr3C2–NiCr coatings on the boiler tube steels using LPG as the fuel gas. *Journal of Materials Processing Technology*. 2006;171(1): 77–82.
38. Singh V, Singla AK, Bansal A. Influence of TiC Content on Slurry Erosion Behaviour of HVOF Sprayed Titanium Carbide and Cupronickel-Chromium Based Coatings. *Journal of Thermal Spray Technology*. 2023;6: 1–9.
39. Uusitalo MA, Vuoristo PM, Mäntylä TA. High temperature corrosion of coatings and boiler steels below chlorine-containing salt deposits. *Corrosion Science*. 2004;46(6): 1311–1331.
40. Agnihotr A, Kalsi SS, Kansal HK, Singh V, Singh H, Handa A. Critical Appraisal of Burnished HVOF Sprayed WCCrC-Ni Coatings against Hot Corrosion in Actual Environmental

Conditions of Coal Fired Boiler. *International Journal of Advanced Science and Technology*. 2020;29(2): 4420–4432.
41. Kim HJ, Lee CH, Hwang SY. Superhard nano WC–12% Co coating by cold spray deposition. *Materials Science and Engineering: A*. 2005;391(1-2): 243–248.
42. Chen L, Wang SQ, Zhou SZ, Li J, Zhang YZ. Microstructure and mechanical properties of Ti (C, N) and TiN/Ti (C, N) multilayer PVD coatings. *International Journal of Refractory Metals and Hard Materials*. 2008;26(5): 456–460.
43. Zhao S, Xie X, Smith GD, Patel SJ. Research and improvement on structure stability and corrosion resistance of nickel-base superalloy INCONEL alloy 740. *Materials & Design*. 2006;27(10): 1120–1127.
44. Planche MP, Normand B, Liao H, Rannou G, Coddet C. Influence of HVOF spraying parameters on in-flight characteristics of Inconel 718 particles and correlation with the electrochemical behaviour of the coating. *Surface and Coatings Technology*. 2002;157(2–3): 247–256.
45. Guo X, Planche MP, Chen J, Liao H. Relationships between in-flight particle characteristics and properties of HVOF sprayed WC-CoCr coatings. *Journal of Materials Processing Technology*. 2014;214(2): 456–461.
46. Kong G, Zhang D, Brown PD, McCartney DG, Harris SJ. Microstructural characterisation of high velocity oxyfuel thermally sprayed Stellite 6. *Materials Science and Technology*. 2003;19(8): 1003–1011.
47. Sundararajan T, Kuroda S, Itagaki T, Abe F. Steam oxidation resistance of Ni-Cr thermal spray coatings on 9Cr-1Mo steel. Part 1: 80Ni-20Cr. *ISIJ International*. 2003;43(1): 95–103.
48. Ma N, Zhang K, Yin D, Zhao D, Zhu Z, Ye F. Synthesis and Characterization of Nanostructured WC-Co/Al Powder Prepared by Mechanical Alloying. *Journal of Nanomaterials*. 2016;2016: 9080684.
49. Sidhu TS, Prakash S, Agrawal RD. Studies of the metallurgical and mechanical properties of high velocity oxy-fuel sprayed stellite-6 coatings on Ni-and Fe-based superalloys. *Surface and Coatings Technology*. 2006;201(1-2): 273–281.
50. Kalsi SS, Sidhu TS, Singh H, Karthikeyan J. Behavior of cold spray coating in real incineration environment. *Materials and Manufacturing Processes*. 2016;31(11): 1468–1475.
51. Kalsi SS, Sidhu TS, Singh H, Karthikeyan J. Analysis of material degradation for uncoated and NiCoCrAlY cold spray coated Superfer 800H in the secondary chamber of medical waste incinerator. *Engineering Failure Analysis*. 2014;(46): 238–246.
52. Dent AH, Horlock AJ, McCartney DG, Harris SJ. Microstructural characterisation of a Ni-Cr-BC based alloy coating produced by high velocity oxy-fuel thermal spraying. *Surface and Coatings Technology*. 2001;139(2–3): 244–250.
53. Singh H, Sidhu TS, Kalsi SB. Behaviour of cold sprayed superalloy in incinerator at 900°C. *Surface Engineering*. 2015;31(11): 846–852.
54. Singh H, Sidhu TS, Karthikeyan J, Kalsi SB. Evaluation of characteristics and behavior of cold sprayed Ni–20Cr coating at elevated temperature in waste incinerator plant. *Surface and Coatings Technology*. 2015;261: 375–384.
55. Somasundaram B, Kadoli R, Ramesh MR. Evaluation of Thermocyclic Oxidation Behavior of HVOF Sprayed WC-CrC-Ni Coatings. *Bonfring International Journal of Industrial Engineering and Management Science*. 2015;5(2): 83–89.
56. Selvam Kevin P, Tiwari A, Seman S, Beer Mohamed SA, Jayaganthan R. Erosion-corrosion protection due to Cr3C2-NiCr cermet coating on stainless steel. *Coatings*. 2020;10(11): 1042.

THE AUTHORS

Atul Agnihotri
e-mail: er.atul84@gmail.com

Kalsi S.B.S.
e-mail: kalsi_asr@yahoo.com

Harmesh Kansal
e-mail: harmeshkansal@gmail.com